

Mesenchymal Stem Cell Mechanics from the Attached to the Suspended State

John M. Maloney,[†] Dessy Nikova,[†] Franziska Lautenschläger,[¶] Emer Clarke,^{||} Robert Langer,^{‡§} Jochen Guck,[¶] and Krystyn J. Van Vliet^{†§*}

[†]Department of Materials Science and Engineering, [‡]Department of Chemical Engineering, and [§]Department of Biological Engineering, Massachusetts Institute of Technology, Cambridge, Massachusetts; [¶]Department of Physics, Cavendish Laboratory, University of Cambridge, Cambridge, United Kingdom; and ^{||}ReachBio, Seattle, Washington

ABSTRACT Human mesenchymal stem cells (hMSCs) are therapeutically useful cells that are typically expanded in vitro on stiff substrata before reimplantation. Here we explore MSC mechanical and structural changes via atomic force microscopy and optical stretching during extended passaging, and we demonstrate that cytoskeletal organization and mechanical stiffness of attached MSC populations are strongly modulated over >15 population doublings in vitro. Cytoskeletal actin networks exhibit significant coarsening, attendant with decreasing average mechanical compliance and differentiation potential of these cells, although expression of molecular surface markers does not significantly decline. These mechanical changes are not observed in the suspended state, indicating that the changes manifest themselves as alterations in stress fiber arrangement rather than cortical cytoskeleton arrangement. Additionally, optical stretching is capable of investigating a previously unquantified structural transition: remodeling-induced stiffening over tens of minutes after adherent cells are suspended. Finally, we find that optically stretched hMSCs exhibit power-law rheology during both loading and recovery; this evidence appears to be the first to originate from a biophysical measurement technique not involving cell-probe or cell-substratum contact. Together, these quantitative assessments of attached and suspended MSCs define the extremes of the extracellular environment while probing intracellular mechanisms that contribute to cell mechanical response.

INTRODUCTION

Potential therapeutic applications abound for a minor cell subpopulation of adult bone marrow stroma often termed mesenchymal stem cells (MSCs) (1). These primary cells have been explanted, expanded in culture, and deployed in clinical trials for conditions including osteogenesis imperfecta (2), myocardial infarction (3), and other pathologies that would benefit from mesenchymal tissue repair. MSCs are generally separated from other cells within the bone marrow stroma by density centrifugation and then seeded upon tissue culture polystyrene (TCPS) (4); indeed, attachment and rapid proliferation on a rigid substratum partially define MSCs (5). Human MSCs (hMSCs) are also defined by expression or lack thereof of certain surface epitopes (e.g., CD73⁺, CD105⁺, CD34⁻, and CD45⁻), which are usually characterized by fluorophore-conjugated antibody tagging, and finally by their ability to differentiate into several downstream lineages such as adipocytes, chondrocytes, and osteoblasts via chemical induction (1). Recent work has advanced our knowledge considerably about the influence of external mechanical cues on population phenotype (6,7). In particular, long-term culturing on rigid substrata leads inevitably to decreased growth rate and eventual senescence, attendant with decreased differentiation propensity and telomere length (8–10). These common features notwithstanding, MSCs compose a heterogeneous

mixture of subpopulations with differing morphologies, proliferation rates, and presentation of cytoskeletal stress fibers (4,11,12), along with possible mechanical differences.

Our goal is to identify and characterize hMSC mechanical markers (as opposed to biomolecular or biochemical markers) that might elucidate cellular mechanisms and population transformations. We hypothesize that MSC population mechanics may be altered by extended in vitro passaging. MSCs are generally expanded in colonies on TCPS, and this rigid substratum material provides a favorable anchor for mechanical testing of individual cells. However, there is also motivation to characterize these adherent cells in the suspended state, which represents not only the alternate extreme of the mechanical extracellular environment relevant to cell delivery, but also a new setting for investigating stem cell mechanics. (By “adherent”, we mean having a tendency to attach to substrata if possible.) We have therefore designed our study to employ two techniques, atomic force microscopy (AFM) and optical stretching (OS), to identify and investigate mechanical markers of single primary MSCs in the attached and suspended states, respectively (see Fig. 1 and Materials and Methods for an overview of these techniques). In general, cell stiffness is correlated with greater filamentous actin (F-actin) content and organization in both attached and recently suspended cells (13–16). While AFM can measure both stress fiber and cortical properties, OS primarily measures the deformability of the cortex alone because stress fibers are absent in the suspended state (15). To our knowledge, neither tool has

Submitted May 11, 2010, and accepted for publication August 20, 2010.

*Correspondence: krystyn@mit.edu

Editor: Michael Edidin.

© 2010 by the Biophysical Society
0006-3495/10/10/2479/9 \$2.00

doi: 10.1016/j.bpj.2010.08.052

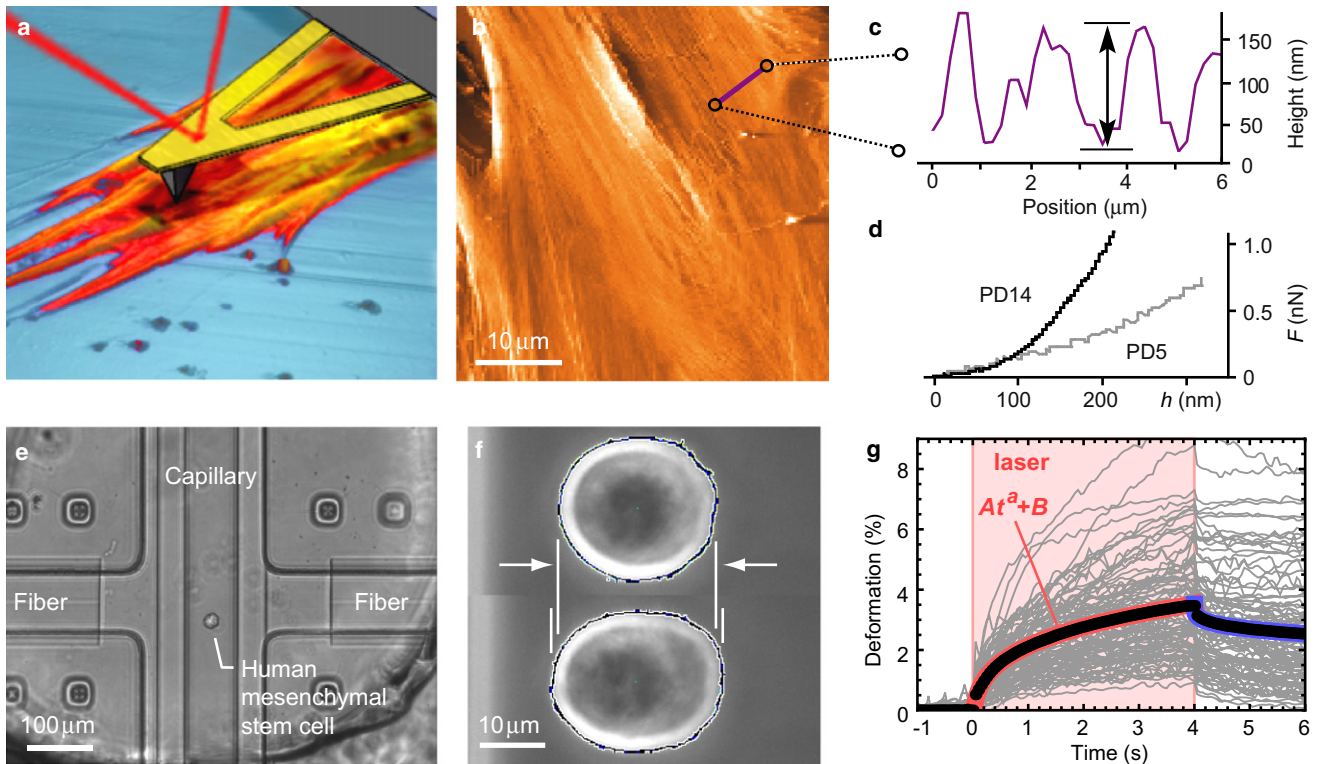


FIGURE 1 Atomic force microscopy (AFM) and optical stretching (OS) allow comparison of adherent cell mechanics in the attached and suspended states. (*a–d*) AFM profiling and indentation quantify cytoskeletal fiber size and cytoskeletal stiffness. (*a*) Schematic of AFM operation in liquid on attached live cells (adapted from (52)). (*b*) Deflection scan of live mesenchymal stem cells (MSCs). (*c*) Cytoskeletal fiber height as characterized by topographical feature height; (*d*) measurement of local stiffness by indentation at two different population doubling (PD) values. (*e–g*) OS measures the stiffness of adherent cells in suspension, absent physical contact and direct influence of substratum chemomechanical properties. (*e*) Phase contrast photograph of opposing optical fibers positioned to face a hollow glass capillary filled with cell suspension during operation. (*f*) Edge detection of cell shape with machine vision before (*top*) and during (*bottom*) irradiation; the deformation of the cell diameter along the laser beam axis is used to quantify cell compliance. (*g*) From one passage of human MSCs (PD6, 98 cells), shaded lines show individual cell deformation in response to a step increase and decrease in laser power. Solid markers show average MSC deformation for all PDs, 1288 cells. Behind markers are offset-power-law fits (e.g., $At^a + B$; see Eq. 2) for the stretching and recovery periods, respectively.

yet been applied to track mechanical changes in MSC populations during long-term stem cell expansion over many population doublings (PDs), nor have these tools previously been combined to assess attached and suspended states in the same cell population.

Because OS is the less prominent of these two techniques, we are also interested in demonstrating previously unrecognized capabilities in this study of cell mechanical markers. One example is the investigation of the suspended state, which was characterized morphologically several decades ago (17–19) but has remained largely uninvestigated since then, despite featuring fascinating cellular mechanisms such as nonapoptotic dynamic blebbing (20,21). Another example is the resolution of a discrepancy in reports of weak power-law rheology (PLR). This constitutive behavior is characterized by scale-free deformation (22–25) and has been studied via numerous contact techniques; Lenormand et al. (26) summarized PLR findings up to 2008, and recent studies have observed PLR behavior by using micropipette aspiration (27), optical tweezers (28), and AFM (29–33). However, a previous OS investigation rejected the PLR

model for suspended cells in favor of a spring-dashpot model with a characteristic relaxation time (34,35), and we revisit that evidence and conclusion with the considerably larger data set (>1200 independently measured cells) acquired in this study.

The complementary advantages of AFM and OS favor their combined use for studying attached and suspended MSCs with a focus not only on characterizing therapeutically useful cells for possible sorting and/or diagnostic applications, but also on investigating fundamental cellular mechanisms such as remodeling after detachment and cell rheology. In the current work, primary human and porcine MSCs were expanded over sequential passages on TCPS. The nanoscale topography of living MSCs was assessed with contact-mode AFM, and the average cell stiffness over stress fibers was determined from AFM-enabled indentation. Structural and mechanical adaptations over multiple PDs were compared with defined molecular markers assessed via flow cytometry and with differentiation potential assessed via standard osteogenesis and adipogenesis protocols. The cytoskeletal arrangement and F-actin bundle radius and stiffness between

different passages were compared via AFM on >300 cells. Furthermore, an optical stretcher augmented with syringe rotation was used to examine >10,000 cells, and to generate creep compliance measurements in stretching and recovery of >1200 cells. These two techniques have allowed us to detect alterations in MSC mechanics initiated by external cues over multiple timescales, from structural and mechanical changes over months of *in vitro* passaging, to cell remodeling over tens of minutes after detachment from a rigid substratum, to characteristic deformation occurring over seconds from an applied photonic load.

MATERIALS AND METHODS

Detailed protocols can be found in the [Supporting Material](#). Human MSCs were analyzed over 17 PDs, representing approximately eight passages after bone marrow isolation and colony identification. Local cytoskeletal mechanical deformability was characterized, and attached cell morphology studied, by profiling and indenting attached living hMSCs via AFM, which can interrogate the F-actin geometry and the local mechanical stiffness of attached cells ([Fig. 1a–d](#)). Briefly, stress fiber radius was approximated by the bundle height in AFM height profiles acquired in contact mode, rather than the apparent width, to minimize shape convolution of the probe (25 nm radius) and actin fibers. Phalloidin staining of chemically fixed hMSCs confirmed that the cytoskeletal networks visible in AFM images consisted primarily of F-actin concentrated densely about the nucleus and in the form of stress fibers ([Fig. S1](#) in the [Supporting Material](#)). As described in the [Supporting Material](#), elastic moduli were estimated via AFM-enabled indentation according to the Hertzian-based model for a spherical indenter, where the relationship between applied force F and indentation depth δ is given by

$$F = 4E\delta^{3/2}\sqrt{R}/3(1 - \nu^2), \quad (1)$$

where E is elastic modulus and ν is Poisson's ratio (assumed to be 0.5) of the deformed volume (assuming the probe material to be comparably rigid) for maximum indentation depths of 20 nm. The reported stiffness E is not intended to be a rigorous measure of the elastic modulus of an entire cell, but provides a quantitative comparison of the local stiffness among cells or cell populations. Our presentation of stiffness data in terms of mean value and standard error of the mean enables conclusions to be drawn between different passages, despite the fact that the stiffness of cells measured by AFM can vary considerably depending on whether the cells are probed in areas of higher or lower stress fiber concentration (36).

Whole-cell mechanical deformability was characterized, and suspended cell morphology was studied on suspended hMSCs via OS, which evaluates whole-cell mechanics in the suspended state as measured by creep compliance. (MSCs are adherent cells, routinely expanded while attached to substrata that can be detached by methods such as trypsinization for study in the suspended state.) Dual counterpropagating laser beams attract and center a single suspended cell, which deforms by outward photon-induced surface stress due to the change in refractive index at the cell edge (15). The cell response is typically characterized by its deformation along the laser axis as a function of time ([Fig. 1e–g](#)).

Of the constitutive models fitted to the OS data and compared by adjusted r^2 or Akaike Information Criterion (AIC) value, the best fit was acquired with the offset power law

$$\bar{\epsilon}(t) = At^{a_s} + B \quad (0.5 \leq t \leq 4s), \quad (2a)$$

$$\bar{\epsilon}(t) = \bar{\epsilon}(4s) - C(t - 4s)^{a_r} \quad (4 < t \leq 6s), \quad (2b)$$

where $\bar{\epsilon}(t)$ is average deformation, t is time, A and C are the fitted prefactors, and a_s and a_r the exponents for stretching and recovery, respectively,

and B is an offset constant. The standard errors in these fitted parameters were determined via bootstrapping, as detailed in the [Supporting Material](#). The fitted stretching and recovery exponents were similar, as discussed in the text; therefore, for several comparisons in this work, the exponent was fitted with the constraint that $a_s = a_r = a$ (i.e., one exponent was fitted to pooled stretching and recovery data). In the [Supporting Material](#), we also discuss the necessary modifications to implement OS of hMSCs, our observations regarding hMSC morphology and deformation behavior, and the advantages and limitations of OS in analyzing these primary cells.

All values are expressed as mean \pm SE unless otherwise noted. In hypothesis testing, $p < 0.05$ was considered statistically significant and is denoted by an asterisk (*) in figures.

RESULTS

AFM identifies mechanical markers altered by extended passaging

Via AFM, we detected characteristic mechanical and structural markers of hMSCs that changed during *in vitro* expansion on TCPS ([Fig. 2a](#) and [b](#)). Multiple mechanical and structural alterations were detected over 17 population doublings (PDs), including coarsening of the cytoskeleton, increased stress fiber radius, and increased stiffness. AFM images of living hMSCs indicated that cytoskeletal actin fibers, initially concentrated around the nucleus, coarsened via increased bundling over 17 PDs *in vitro*, and appreciable increases in fiber radius were also readily apparent ([Fig. 2a](#)). A fivefold increase in local cytoskeletal stiffness was correlated with increased volume fraction of bundled cytoskeletal actin, as nominal fiber radius increased from 100 to 500 nm ([Fig. 2b](#), $p < 10^{-9}$ by comparing youngest and oldest PD values as described in the [Supporting Material](#)). These same trends of cytoskeletal coarsening were observed in porcine MSCs expanded for 13 PDs on TCPS (see [Fig. S2](#)). Mechanical and structural changes in attached hMSCs were accompanied by a reduction in adipogenic and osteogenic differentiation potential after chemical induction, as consistent with previous studies of reduced differentiation potential upon extended passaging (4,8–10) (see [Fig. S3](#)).

In contrast to the mechanical changes discovered by AFM on attached hMSCs, no passage-dependent trend in mechanical stiffness or creep behavior was observed for suspended hMSCs (from the same donor and two additional donors), as characterized by three independent parameters measured by OS (maximum deformation at the end of the stretching period, recovery multiplicative constant C , and overall power-law exponent a , as shown in [Fig. 2c](#), $p > 0.05$). Expression of the hMSC markers SH2 (CD105) and SH4 (CD73), as quantified by flow cytometry, also did not change considerably over these PDs ([Fig. 2d](#), $p > 0.05$).

hMSCs effectively stiffen over first hour in suspension in response to detachment

Across all passages, the whole-cell compliance of suspended hMSCs (as measured by OS) decreased within the

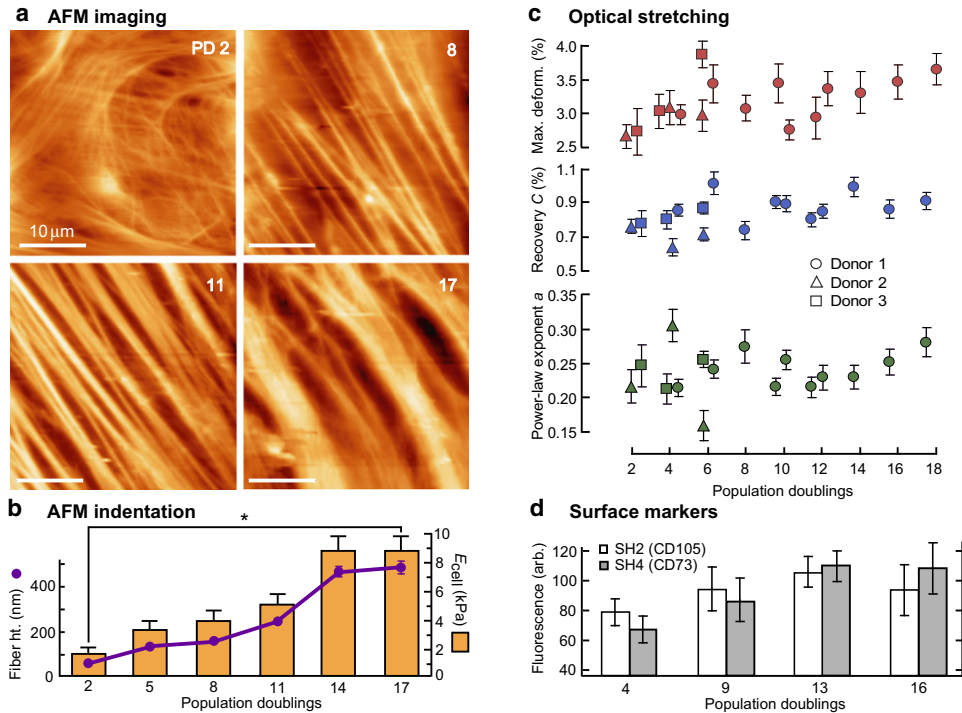


FIGURE 2 Characterization of hMSC cytoskeletal structure and mechanics, chemical surface markers, and whole-cell mechanics over multiple PDs in vitro. (a) AFM deflection-images of hMSCs show cytoskeletal coarsening with increasing culture time in vitro. (b) Cytoskeletal fiber height (representing fiber radius) and cell stiffness as measured by AFM topography images and indentation responses, respectively, are well correlated and increase significantly with passaging ($p < 10^{-9}$, $n = 50$ cells per PD). However, (c) suspended hMSC mechanical parameters as measured by OS (maximum deformation, recovery magnitude C , and overall power-law exponent a , $n = 39$ to 204 cells per PD) and (d) characteristic hMSC surface markers as measured by flow cytometry are minimally changed ($p > 0.05$). (All data shown as mean \pm SE.)

cell population during the first hour of the experiment (starting 30 min after the cells were detached from the TCPS substratum) before reaching an equilibrium value (Fig. 3 a). The rate of stiffening during the first hour was calculated by linear regression to be -1.0 ± 0.3 percent deformation per hour. Other values such as the recovery multiplicative constant C and the overall power-law exponent a did not change observably during this time frame, however. This contrast is also shown in the time frame of the stretching event, where the difference is seen to accumulate during stretching but is unaffected by the laser power reduction to trapping level (Fig. 3 a, inset).

An experiment was performed to decouple the loss of temperature and pH control from substratum detachment, to see whether one or the other was necessary to cause whole-cell stiffening (Fig. 3 b). Cells were either 1), removed from the incubator, kept at room temperature and atmosphere for 1 h, detached, and stretched; or 2), detached, stored in suspension in an incubator for 1 h with the container periodically inverted to counteract cell sinking, and stretched. Whole-cell stiffening was still observed in the population that was kept at room temperature before detachment ($p = 0.02$ for different population deformability), but was not observed in the cells that were stored after detachment ($p = 0.79$ for different population deformability); this population had already equilibrated at a higher average stiffness (i.e., lower maximum deformation). The combination of detachment and subsequent suspension was therefore found to be a necessary stimulus for stiffening of suspended hMSCs over tens of minutes.

Suspended hMSCs exhibit power-law rheology in both stretching and recovery

The average deformation profile from all cells ($n = 1288$) was well fit by an offset-power-law, as illustrated by the fitted average deformation shown in Fig. 1 g and the deformation rate magnitude shown in Fig. 4, where the slope of $|\partial \bar{\epsilon}(t)/\partial t|$ on a log-log scale corresponds to $a-1$. Notably, this power-law behavior is observed both in stretching and recovery and while the cells are fully suspended in the absence of physical contact.

According to our parameterization, the values of A , B , and C were 3.45 ± 0.28 , -1.32 ± 0.27 , and 0.79 ± 0.01 , respectively—with standard errors estimated by bootstrapping, which was found to be a useful way of obtaining the error in a fitted output parameter even in cases where the individual cell responses exhibit considerable noise and are not suitable for fitting (Fig. S4). An offset constant was considered for the recovery period, but its fitted value (0.017 ± 0.001) was found to be negligible compared to the other parameters.

The exponents a_S and a_R were 0.25 ± 0.02 and 0.28 ± 0.01 for the stretching and recovery periods, respectively. The recovery exponent appears to be larger than the stretching exponent, but we cannot rule out this difference being due to chance ($p = 0.08$). If the entire stretching and recovery response is modeled with a single exponent, the response can be described with four parameters: the stretching multiplicative and additive constants, the recovery multiplicative constant, and a single exponent $a = 0.256 \pm 0.005$. This fit to an offset power law was better than a fit to a four-element

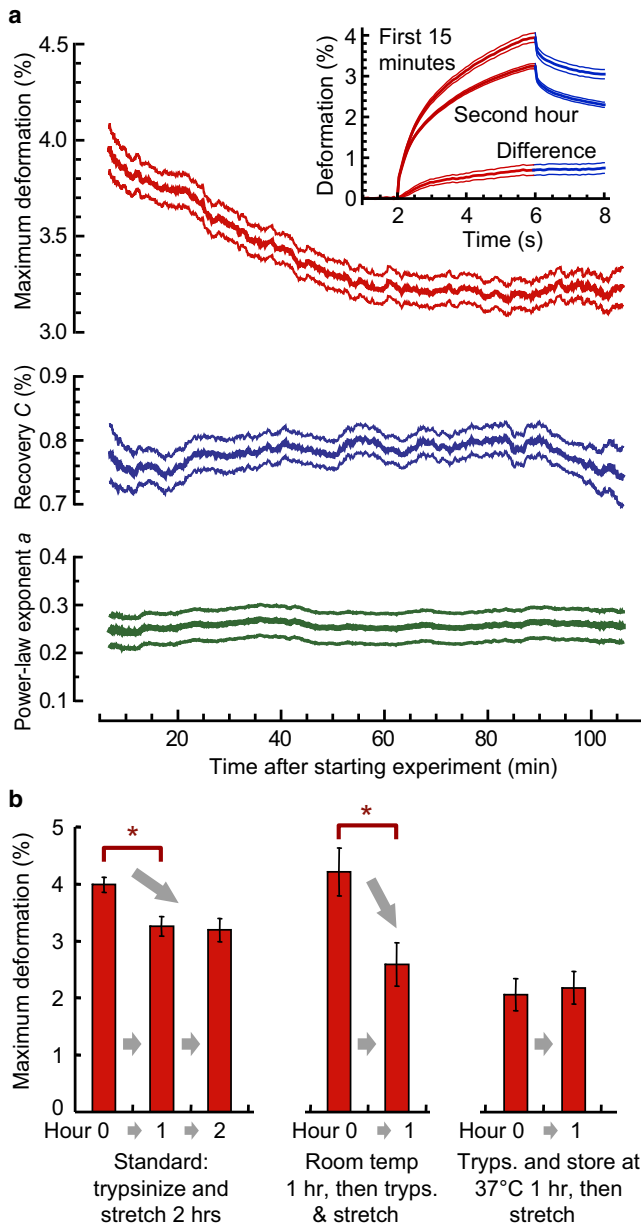


FIGURE 3 Recently suspended cells stiffen after detachment. (a) hMSC compliance, quantified as the average deformation at the end of the stretching period, decreases during the first hour of the stretching experiment (i.e., the time period 30–90 min after detachment) before reaching equilibrium in the second hour (400-cell moving average). (Inset) Accumulated difference in deformation between cells stretched in the first 15 min of the experiment ($n = 232$ cells) and cells stretched in the second hour ($n = 581$ cells) over the stretching and recovery periods. The recovery parameter C and overall power-law exponent a are relatively unaffected during the same time period. (b) Substratum detachment and suspension, but not exposure to room temperature and uncontrolled pH, is necessary for stiffening to occur; cells that were stored in the suspended state at 37°C for 1 h have already equilibrated at higher stiffness when the stretching experiment begins (labeled as Hour 0 for all conditions). (All data shown as mean \pm SE; $p = 0.0009, 0.02,$ and 0.79 for first-hour stiffening for the three conditions, respectively, in panel b.)

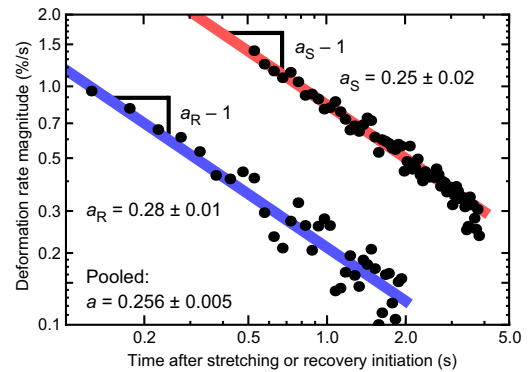


FIGURE 4 Suspended cells exhibit power-law rheology, as measured by noncontact OS. Average hMSC deformation during both stretching (upper line) and recovery (lower line) regimes is well fit by an offset power law (Eq. 2) with stretching and recovery exponents a_S and a_R ($p = 0.08$ for significantly different values) or a single overall exponent a from pooled stretching and recovery data ($n = 1288$ cells); the slope of deformation rate magnitude versus time on a log-log scale is correspondingly $a - 1$. The use of deformation rate instead of deformation eliminates the complicating influence of an offset that manifests itself during the first 0.5 s of stretching. Standard errors are determined by using the bootstrapping technique, as described in the Supporting Material.

viscoelastic model (a spring-dashpot series unit in series with a spring-dashpot parallel unit), as measured by r^2 and AIC comparison (adjusted $r^2 = 0.999995$ vs. 0.998 , or AIC = 1030 vs. -348). Other viscoelastic models, including a three-element model consisting of a dashpot in series with a spring-dashpot parallel unit, scored even worse. To check whether the better fit of the offset-power-law model was possibly due to chance, we performed this comparison 1000 times while resampling the data with the bootstrap technique. The offset-power-law model had a higher adjusted r^2 value and lower AIC each time, indicating that the better fit of this model is unlikely to be due to chance ($p < 0.001$).

DISCUSSION

Mechanical and structural markers of extended passaging exist for hMSCs in the attached state only

We identified mechanical markers that correlate with hMSC phenotype during extended passaging, to complement functional and molecular tests such as chemically induced differentiation and determination of telomere length. Significant cytoskeletal coarsening and stiffening in attached human and porcine primary MSC populations, as measured by AFM, are attendant with reduction in population differentiation capacity. Importantly, these changes are not associated with any detectable changes in selected surface marker expression as measured by flow cytometry or in whole-cell deformability as measured by OS.

The observed reduction in hMSC differentiation potential and eventual loss of proliferative ability is in agreement with

previous reports of *in vitro* culture (4,8–10). Multiple surface markers that are associated with hMSCs are changed minimally (by 20% at most) during extended passaging (10,37), and marker expression decreases considerably only when the entire culture enters senescence (38). In agreement with these studies, here we found no observable change in the expression of putative MSC-positive markers CD105 or CD73 over 12 PDs while the hMSCs were still proliferating.

Multiple MSC subpopulations have long been known to exist (4,11,12), the two most prominent of which are rapidly proliferating spindle-shaped cells and slowly proliferating round or cuboidal cells (39,40). The more rapidly dividing cells exhaust their proliferative capacity relatively early, resulting in an increased proportion of cuboidal cells over time (11). Docheva et al. (40) previously found no distinctive mechanical differences in the (peri)nuclear region of spindle-shaped and cuboidal cells; however, it is not this region but rather in the expression of stress fibers away from the nucleus that morphologically distinguishes these cells: spindle-shaped cells feature a more diffuse, unaligned collection of stress fibers, while cuboidal cells feature abundant pronounced fibers (11,40). Our AFM images of cytoskeletal structure in living hMSCs correlate well with these differences in observed subpopulation morphology.

We conclude, therefore, that our measurements of increasing average stress fiber radius and stiffness across all MSCs with extended passaging represent the mechanical component of a transition from cultures of predominantly spindle-shaped cells to predominantly cuboidal cells. Both subpopulations express surface markers essentially equally under optimal conditions (10,37); however, the cuboidal cells are less likely to differentiate down any lineage other than osteoblastic (41), and thus the entire population exhibits reduced adipogenic and chondrogenic capability with extended passaging. We highlight the finding that this loss of population differentiation potential appears better correlated and more dramatically apparent with average MSC stiffness (measured on attached cells over stress fibers) than with surface marker presentation.

We also note the contrast between the finding of mechanical alterations in the attached state (by AFM) and the absence of detectable changes in the suspended state (by OS), even when the suspended cells were attached to TCPS only some tens of minutes before beginning each OS experiment. It is important to note that cell detachment does not erase the passaging-dependent mechanical stiffening trend found with AFM, as all MSCs were detached every other PD for passaging. Evidently, no correlation is seen with OS because the predominant cytoskeletal changes are manifested only in the attached state. We conclude that MSC population aging is structurally characterized by considerable changes in stress fiber organization but minimal changes in cortical actin organization. Our conclusion is compatible with the finding of Darling et al. (42) that

mechanical differences lessened between MSCs and cells representing their downstream lineages when the cells were barely attached. Structural contrasts between different lineages/passages that arise with attachment and spreading (and disappear with detachment) are expected if stress fiber organization is readily altered by differentiation/passaging while total actin content and cortical thickness and organization is not readily altered. We do not suggest that all measurable mechanical differences vanish when adherent cells are suspended; differences in cancer cells and chemically differentiated cells have in fact been found in the suspended state (16,43). However, differences that manifest themselves primarily in altered morphology and mechanical properties of stress fibers, which appear only in attached cells, may be difficult or impossible to detect while the cells are suspended.

Effective stiffening of recently suspended hMSCs correlates with cortex-membrane remodeling and stabilization

The stiffening we observed 30–90 min after hMSC detachment (subsequent to a presumed reduction in stiffness when stress fibers depolymerized during trypsinization) represents another mechanical transition, one acting on a much shorter timescale than the passaging-induced effects. This transition could conceivably originate from the detachment process or from extended time at room temperature and pH uncontrolled by the CO₂-bicarbonate buffer system during OS experiments. We found from decoupling these two conditions that it is prolonged suspension for tens of minutes that triggers hMSC stiffening over this timescale. It is possible that actin made available from stress fiber depolymerization is incorporated into the actin cortex, but we would expect to observe stiffening both in stretching and recovery if this mechanism were dominant. Instead, the cells effectively stiffen only in stretching, suggesting that an asymmetric process such as molecular unbinding occurs. Over the same timescale we observed a significant reduction in blebbing (see the [Supporting Material](#)), in agreement with literature reports of surface remodeling and blebbing reduction in multiple cell lines over tens of minutes after detachment (17–19). It is known that the plasma membrane provides a reservoir of surface area that adapts to the changing needs of the cell during suspension and attachment (44); in general, cells that are initially more spread out upon substrata exhibit more blebs in suspension after detachment (45) as the cells assume a spherical shape. It has recently been reaffirmed that cell rounding induces cortex-membrane destabilization (21).

We propose that these two correlated temporal processes (stiffening and blebbing reduction) are connected, and that the remodeling process (predominantly, the reattachment and strengthening of cytoskeletal-membrane links) stiffens the suspended cell. It would follow first that a certain

amount of bond detachment occurs between the membrane and actin cortex during stretching (but not recovery, due to minimal or absent driving force), and second that bond strength and/or density increases with increasing time since cell detachment from the substratum. This explanation is compatible with the significantly lower percentage of blebbing cells observed after some time in suspension, and with the previous literature reports on cell remodeling, heretofore unquantified in terms of resulting mechanical stiffness changes. Further study is needed, however, to determine which cytoskeletal components and connections dominate in this transition, and whether effective stiffening, putatively cortex-membrane reconnection, of recently suspended cells has any influence on therapeutic applications involving injection of suspended hMSCs and their subsequent extravasation and migration *in vivo*.

Power-law rheology characterizes suspended cells and recovery after loading

In the process of accumulating hMSC creep data from different passages and donors via OS, we have found that weak power-law rheology (PLR) applies to cells in the suspended state and furthermore to cells undergoing creep recovery, with the best fitting constitutive law expressed by Eq. 2. The fitted values and standard error of the exponents are $a_S = 0.25 \pm 0.02$ and $a_R = 0.28 \pm 0.01$ for stretching and recovery, respectively, or pooled as $a = 0.256 \pm 0.005$. As noted previously, the larger a_R is not statistically different from a_S at the 5% significance level ($p = 0.08$).

We first focus on the finding of power-law behavior in suspended cells by a noncontact technique, which extends and is compatible with many studies in the literature that have explored the dependency of PLR on the presence of certain cytoskeletal components. Other groups have applied cytoskeletal inhibitors to reduce stress fibers and inhibit actomyosin contraction (46), decoupled attachment mechanisms by attaching probes with various molecular linkers to engage an assortment of transmembrane receptors (24,25), and minimized adhesion to reduce the formation of features such as focal adhesions and stress fibers by testing cells on relatively inert poly(HEMA) coatings (30) and with micropipette aspiration (27). Cells under all of these conditions have exhibited power-law behavior. Our study takes the avoidance of contact effects, stress concentrations, and focal adhesions to its limit; during OS, our hMSCs are totally suspended and engaged with a photonic load only.

Our results serve to correct an earlier report that adherent cells do not exhibit PLR in the suspended state, as measured by OS (34,35), which has since been interpreted as an indication of a fundamental rheological difference between cells in the suspended and attached states (47,48). That study compared r^2 values between a power law and a viscoelastic response and found that the viscoelastic model scored higher. We suggest two possible reasons for the discrepancy

between these two OS results: First, the earlier comparison was performed for a relatively small collection of cells or a single cell only; thus, the better fit to a lumped-component viscoelastic model could have been due to chance. Our larger data set of 1288 cells, along with bootstrap resampling across 1000 iterations, leads us to conclude that the better fit of the power law here is not due to chance. Second, the former viscoelastic model featured three fitted parameters (representing a dashpot in series with a spring-dashpot parallel unit), while the power law featured just two (i.e., $\varepsilon(t) = At^a$). In general, more parameters will produce a better fit, so this comparison does not fairly evaluate the models based on the desirable metric of combined good fit and simplicity. In this work, we have compared models by using as criteria adjusted r^2 and AIC, as these metrics penalize additional terms and therefore enable a more even comparison between models with different numbers of fitted parameters.

Our second focus is the finding of PLR in creep recovery, as such reports are rare in comparison to reports of PLR in creep stretching. A correspondence between power-law exponents has been previously observed for isolated nuclei that were mechanically deformed, then released, by micropipette aspiration (49) and also for attached cells probed by magnetic bead cytometry (50). However, to our knowledge the current results are the first such observations to be reported for suspended whole cells. An increase in power-law exponent has been measured for cells with lower prestress (51); this result is compatible with our finding that the power-law exponent measured on suspended cells, which lack stress fibers, is at the high end of the range (typically 0.10–0.30) of exponents measured on attached cells. It is also intriguing that the negative offset value B is not observed in recovery; possible origins of this offset constant B are discussed in the [Supporting Material](#).

CONCLUSIONS

Our observations of dynamic MSC mechanical markers over different timescales illuminate several previously unexplored areas involving stress fiber participation in cell mechanics, and are also largely consistent with existing MSC and cell rheology literature. We view a newly explanted MSC population as a heterogeneous mixture of cells that proliferate rapidly on stiff substrata. As subpopulations enter senescence at different timepoints, population profile changes are observable partly through cytoskeletal coarsening and stiffening. Our contribution has been to quantify the mechanics of this transition and show its dependence on stress fiber presentation: fivefold stiffening of attached MSCs is observed in the typical conditions for *in vitro* expansion and subsequent study. Such mechanical changes provide further evidence of altered MSC characteristics during extended passaging on stiff substrata, and may compete with the effects of other stimuli (e.g., cytoskeletal

alteration during chemically induced differentiation). Ultimately, the duration and mechanical environment of MSC expansion should be balanced against these structural, mechanical, and functional adaptations of culture-expanded MSC populations; furthermore, these findings motivate the development of culture conditions that will control or minimize such changes. The absence of corresponding stiffness differences in the suspended state unfortunately hinders efforts to sort MSC subpopulations by stiffness in a high-throughput tool. However, an optimistic finding is the capability of AFM in complement with OS to decouple the mechanical contributions of stress fibers without the need of cytoskeletal inhibitors.

Another intriguing finding is the stiffening of an adherent cell over tens of minutes after being released from substratum contact; correlations with changing cell surface topography (specifically, the reduction of blebbing as membrane-cortex connections develop and strengthen) suggest that we are measuring a previously unquantified mechanical component of cell remodeling. Finally, the noncontact feature of photonic mechanical loading has allowed us to identify power-law rheology in whole cells in the absence of stress fibers, indicating that power-law creep compliance does not depend critically on stress-fiber-generated prestress. We expect this conclusion to be valuable in the refinement of constitutive models of whole-cell deformation that not only predict the emergence of power-law rheology, but also can be related directly to molecular mechanisms.

SUPPORTING MATERIAL

Additional materials and methods, four figures, and one movie are available at [http://www.biophysj.org/biophysj/supplemental/S0006-3495\(10\)01048-9](http://www.biophysj.org/biophysj/supplemental/S0006-3495(10)01048-9).

We gratefully acknowledge Esther Yu's and Kyle Bryson's assistance with AFM and OS experiments, respectively, and Adam Zeiger's and Emilio Silva's assistance in creating the AFM schematic.

This work was supported in part by the Arnold and Mabel Beckman Foundation, National Science Foundation CAREER grant No. CBET-0644846 (to K.J.V.V.), the Human Frontiers Science Program (K.J.V.V. and J.G.), a technology transfer grant from the Cambridge-MIT Institute (to J.G. and K.J.V.V.), the Gates Cambridge Scholarship (to F.L.), and the Molecular, Cellular, Tissue and Biomechanics Training grant No. EB006348 from the National Institutes of Health, National Institute of Biomedical Imaging and Bioengineering (to J.M.M.).

REFERENCES

- Pittenger, M. F., A. M. Mackay, ..., D. R. Marshak. 1999. Multilineage potential of adult human mesenchymal stem cells. *Science*. 284:143–147.
- Horwitz, E. M., D. J. Prockop, ..., M. K. Brennan. 1999. Transplantability and therapeutic effects of bone marrow-derived mesenchymal cells in children with osteogenesis imperfecta. *Nat. Med.* 5:309–313.
- Chen, S. L., W. W. Fang, ..., J. P. Sun. 2004. Effect on left ventricular function of intracoronary transplantation of autologous bone marrow mesenchymal stem cell in patients with acute myocardial infarction. *Am. J. Cardiol.* 94:92–95.
- Bruder, S. P., N. Jaiswal, and S. E. Haynesworth. 1997. Growth kinetics, self-renewal, and the osteogenic potential of purified human mesenchymal stem cells during extensive subcultivation and following cryopreservation. *J. Cell. Biochem.* 64:278–294.
- Dominici, M., K. Le Blanc, ..., E. Horwitz. 2006. Minimal criteria for defining multipotent mesenchymal stromal cells. The International Society for Cellular Therapy position statement. *Cytotherapy*. 8:315–317.
- Engler, A. J., S. Sen, ..., D. E. Discher. 2006. Matrix elasticity directs stem cell lineage specification. *Cell*. 126:677–689.
- Chowdhury, F., S. Na, ..., N. Wang. 2009. Material properties of the cell dictate stress-induced spreading and differentiation in embryonic stem cells. *Nat. Mater.* 9:82–88.
- Banfi, A., A. Muraglia, ..., R. Quarto. 2000. Proliferation kinetics and differentiation potential of ex vivo expanded human bone marrow stromal cells: Implications for their use in cell therapy. *Exp. Hematol.* 28:707–715.
- Bonab, M. M., K. Alimoghaddam, ..., B. Nikbin. 2006. Aging of mesenchymal stem cell in vitro. *BMC Cell Biol.* 7:14.
- Kim, J., J. W. Kang, ..., H. S. Kim. 2009. Biological characterization of long-term cultured human mesenchymal stem cells. *Arch. Pharm. Res.* 32:117–126.
- Mets, T., and G. Verdonk. 1981. In vitro aging of human bone marrow derived stromal cells. *Mech. Ageing Dev.* 16:81–89.
- Colter, D. C., I. Sekiya, and D. J. Prockop. 2001. Identification of a subpopulation of rapidly self-renewing and multipotential adult stem cells in colonies of human marrow stromal cells. *Proc. Natl. Acad. Sci. USA*. 98:7841–7845.
- Petersen, N. O., W. B. McConaughy, and E. L. Elson. 1982. Dependence of locally measured cellular deformability on position on the cell, temperature, and cytochalasin B. *Proc. Natl. Acad. Sci. USA*. 79:5327–5331.
- Rotsch, C., and M. Radmacher. 2000. Drug-induced changes of cytoskeletal structure and mechanics in fibroblasts: an atomic force microscopy study. *Biophys. J.* 78:520–535.
- Guck, J., R. Ananthakrishnan, ..., J. Käs. 2001. The optical stretcher: a novel laser tool to micromanipulate cells. *Biophys. J.* 81:767–784.
- Guck, J., S. Schinkinger, ..., C. Bilby. 2005. Optical deformability as an inherent cell marker for testing malignant transformation and metastatic competence. *Biophys. J.* 88:3689–3698.
- Harrison, C. J., and T. D. Allen. 1979. Cell surface morphology after trypsinization depends on initial cell shape. *Differentiation*. 15:61–66.
- Garnett, H. M. 1980. A scanning electron microscope study of the sequential changes in morphology occurring in human fibroblasts placed in suspension culture. *Cytobios*. 27:7–18.
- Kinn, S. R., and T. D. Allen. 1981. Conversion of blebs to microvilli: cell surface reorganization after trypsin. *Differentiation*. 20:168–173.
- Charras, G. T., M. Coughlin, ..., L. Mahadevan. 2008. Life and times of a cellular bleb. *Biophys. J.* 94:1836–1853.
- Fackler, O. T., and R. Grosse. 2008. Cell motility through plasma membrane blebbing. *J. Cell Biol.* 181:879–884.
- Fabry, B., G. N. Maksym, ..., J. J. Fredberg. 2001. Scaling the micro-rheology of living cells. *Phys. Rev. Lett.* 87:148102.
- Fabry, B., G. N. Maksym, ..., J. J. Fredberg. 2003. Time scale and other invariants of integrative mechanical behavior in living cells. *Phys. Rev. E Stat. Nonlin. Soft Matter Phys.* 68:041914.
- Puig-de Morales, M., E. Millet, ..., J. J. Fredberg. 2004. Cytoskeletal mechanics in the adherent human airway smooth muscle cell: probe specificity and scaling of protein-protein dynamics. *Am. J. Physiol. Cell Physiol.* 287:C643–C654.
- Balland, M., N. Desprat, ..., F. Gallet. 2006. Power laws in microrheology experiments on living cells: Comparative analysis and modeling. *Phys. Rev. E Stat. Nonlin. Soft Matter Phys.* 74:021911.

26. Lenormand, G., A. M. Alencar, ..., J. J. Fredberg. 2008. The cytoskeleton of the living cell as an out-of-equilibrium system. *In Phase Transitions in Cell Biology*. Springer, Dordrecht, The Netherlands. 111–141.
27. Zhou, E. H., S. T. Quek, and C. T. Lim. 2010. Power-law rheology analysis of cells undergoing micropipette aspiration. *Biomech. Model. Mechanobiol.* 10.1007/s10237-010-0197-7.
28. Icard-Arcizet, D., O. Cardoso, ..., S. Hénon. 2008. Cell stiffening in response to external stress is correlated to actin recruitment. *Biophys. J.* 94:2906–2913.
29. Smith, B. A., B. Tolloczko, ..., P. Grütter. 2005. Probing the viscoelastic behavior of cultured airway smooth muscle cells with atomic force microscopy: stiffening induced by contractile agonist. *Biophys. J.* 88:2994–3007.
30. Roca-Cusachs, P., I. Almendros, ..., D. Navajas. 2006. Rheology of passive and adhesion-activated neutrophils probed by atomic force microscopy. *Biophys. J.* 91:3508–3518.
31. Hemmer, J. D., J. Nagatomi, ..., M. Laberge. 2009. Role of cytoskeletal components in stress-relaxation behavior of adherent vascular smooth muscle cells. *J. Biomech. Eng.* 131:041001.
32. Sunyer, R., X. Trepal, ..., D. Navajas. 2009. The temperature dependence of cell mechanics measured by atomic force microscopy. *Phys. Biol.* 6:025009.
33. Hiratsuka, S., Y. Mizutani, ..., T. Okajima. 2009. The number distribution of complex shear modulus of single cells measured by atomic force microscopy. *Ultramicroscopy.* 109:937–941.
34. Wottawah, F., S. Schinkinger, ..., J. Käs. 2005. Optical rheology of biological cells. *Phys. Rev. Lett.* 94:098103.
35. Wottawah, F., S. Schinkinger, ..., J. Guck. 2005. Characterizing single suspended cells by optorheology. *Acta Biomater.* 1:263–271.
36. Lee, S., A. Zeiger, ..., I. M. Herman. 2010. Pericyte actomyosin-mediated contraction at the cell–material interface can modulate the microvascular niche. *J. Phys. Condens. Matter.* 22:194115.
37. Pal, R., M. Hanwate, ..., S. Totey. 2009. Phenotypic and functional comparison of optimum culture conditions for upscaling of bone marrow-derived mesenchymal stem cells. *J. Tissue Eng. Regen. Med.* 3:163–174.
38. Wagner, W., P. Horn, ..., A. D. Ho. 2008. Replicative senescence of mesenchymal stem cells: a continuous and organized process. *PLoS ONE.* 3:e2213.
39. Sekiya, I., B. L. Larson, ..., D. J. Prockop. 2002. Expansion of human adult stem cells from bone marrow stroma: conditions that maximize the yields of early progenitors and evaluate their quality. *Stem Cells.* 20:530–541.
40. Docheva, D., D. Padula, ..., M. Schieker. 2008. Researching into the cellular shape, volume and elasticity of mesenchymal stem cells, osteoblasts and osteosarcoma cells by atomic force microscopy. *J. Cell. Mol. Med.* 12:537–552.
41. Digirolamo, C. M., D. Stokes, ..., D. J. Prockop. 1999. Propagation and senescence of human marrow stromal cells in culture: a simple colony-forming assay identifies samples with the greatest potential to propagate and differentiate. *Br. J. Haematol.* 107:275–281.
42. Darling, E. M., M. Topel, ..., F. Guilak. 2008. Viscoelastic properties of human mesenchymally-derived stem cells and primary osteoblasts, chondrocytes, and adipocytes. *J. Biomech.* 41:454–464.
43. Lautenschläger, F., S. Paschke, ..., J. Guck. 2009. The regulatory role of cell mechanics for migration of differentiating myeloid cells. *Proc. Natl. Acad. Sci. USA.* 106:15696–15701.
44. Erickson, C. A., and J. P. Trinkaus. 1976. Microvilli and blebs as sources of reserve surface membrane during cell spreading. *Exp. Cell Res.* 99:375–384.
45. Rovinsky, Y. A., and J. M. Vasiliev. 1984. Surface topography of suspended tissue cells. *Int. Rev. Cytol.* 90:273–307.
46. Bursac, P., G. Lenormand, ..., J. J. Fredberg. 2005. Cytoskeletal remodeling and slow dynamics in the living cell. *Nat. Mater.* 4:557–561.
47. Pullarkat, P. A., P. A. Fernández, and A. Ott. 2007. Rheological properties of the eukaryotic cell cytoskeleton. *Phys. Rep.* 449:29–53.
48. Hoffman, B. D., and J. C. Crocker. 2009. Cell mechanics: dissecting the physical responses of cells to force. *Annu. Rev. Biomed. Eng.* 11: 259–288.
49. Dahl, K. N., A. J. Engler, ..., D. E. Discher. 2005. Power-law rheology of isolated nuclei with deformation mapping of nuclear substructures. *Biophys. J.* 89:2855–2864.
50. Kollmannsberger, P. 2009. Nonlinear microrheology of living cells. PhD thesis. University of Erlangen-Nürnberg, Germany.
51. Stamenovic, D., B. Suki, ..., J. J. Fredberg. 2004. Rheology of airway smooth muscle cells is associated with cytoskeletal contractile stress. *J. Appl. Physiol.* 96:1600–1605.
52. Ludwig, T., R. Kirmse, ..., U. S. Schwarz. 2008. Probing cellular microenvironments and tissue remodeling by atomic force microscopy. *Pflugers Arch.* 456:29–49.